Electromigration of Au on Ge(111): Adatom and island dynamics

F. Leroy [*], A. El Barraj, F. Cheynis, P. Müller, and S. Curiotto
Aix Marseille Univ., CNRS, CINaM, AMUTECH, UMR CNRS 7325 Case 913 Campus de Luminy, Marseille Cedex 13288, France

(Received 31 May 2022; revised 22 August 2022; accepted 25 August 2022; published 2 September 2022; corrected 21 September 2022)

We have observed the motion of two-dimensional phases of Au on Ge(111) under an electric bias by *in operando* low energy electron microscopy. Electromigration of Au results in a complex dynamics that depends on the nature of the involved mobile phases: two-dimensional adatom gas or two-dimensional islands. We show that the Au adatoms move at the surface in the direction opposite to the electric current. The wind force induced by the electron flow is measured: the effective valence of Au ($Z^* = -82 \pm 15$) is directly deduced from the coverage profile of a Au adatom gas spatially retained by a strong Erlich-Schwoebel barrier at a downhill step edge. The velocity of two-dimensional Au islands versus island size reveals a mass transport by terrace diffusion inside the islands. The energy barrier for diffusion above 820 K is 1.16 ± 0.08 eV and it strongly increases up to 3.1 ± 0.6 eV below. We attribute this change of regime to a modification of diffusing species from single Au atoms at high temperature to Au clusters at low temperature. The strong shape fluctuations of the 2D islands is consistent with a nearly vanishing line tension of 1.2 ± 0.4 meV/nm at 800 K.

DOI: 10.1103/PhysRevB.106.115402

I. INTRODUCTION

Mass transport phenomena occurring at solid surfaces are crucial in the context of nanofabrication and growth processes. To study these phenomena one approach consists of analyzing the fluctuation dynamics of surface structures such as island edges [1–3] or their response to a perturbation [4]. In that respect mass transport induced by an electric current [5–7] provides a unique opportunity to study atomic processes using the electric current as a perturbation of the random processes occurring at the surface [8–11]. For instance the size dependence of the velocity of 2D islands that are displaced by a flowing electric current is intimately related to the atomic processes of diffusion and attachment-detachment at step edges [12–14]. If there is a key benefit of studying a directed motion rather than a random motion from a statistical analysis point of view, the counterpart is to know quantitatively the applied force. Historically electromigration has been studied in solids and thin films [6,7,15–17]. It has been proposed that the driving force for atom migration arises from two sources: (i) the external electric field acts directly on the partially charged atoms and the driving force is called the direct force; (ii) the electric current carriers transfer a momentum to the atoms, and this results in a driving force called the wind force [18–20]. The experimental determination of the dominant force and the quantification of the effective adatom valence are still very rare [8] and call for dedicated studies [6,7]. In addition electromigration phenomena of adatoms at surfaces [6,7,17–22] can cause substantial changes in the surface morphology such as step bunching for vicinal surfaces [15,16,23,24] or shape instabilities of 2D islands [4,9,25–27]. These surface modifications are also intimately related to the dominant mass transport phenomenon.

This article aims at addressing the mechanisms of Au transport on Ge(111), i.e., the diffusivity of Au, the energy barriers involved in mass transport, as well as the effective valence of the adatoms. In that purpose, and to disentangle the different terms that are involved in the electromigration process, the results rely on the analysis of the migration phenomena of two-dimensional (2D) layers of Au in different states: gas, Au-rich and Au-poor 2D islands. This study is based on an *in operando* observation under an electric current of the Au-Ge(111) surface by low energy electron microscopy (LEEM). The experimental setup allows us to study the spatiotemporal dynamics at a surface [28,29]. At high temperature (above ~800 K) using the 2D adatom gas coverage profile nearby a step edge we determine the effective valence of Au adatoms at the Ge(111) surface responsible for the wind force ($Z^* = -82 \pm 20$). Decreasing the temperature the gas phase condenses into a 2D dilute phase of Au (Au-poor phase) and forms 2D islands on Ge(111). The electromigration velocity of these islands versus the island size indicates a mass transport phenomenon limited by terrace diffusion inside the islands. In addition the large fluctuations of the island edges indicate a vanishingly small line tension of 1.2 ± 0.4 meV/nm at 800 K. At even lower temperature (or higher Au coverage) a dense Au-rich phase forms that is comparatively immobile. The apparent migration of this phase is induced by phase transformation with the surrounding Au-poor phase and is limited by mass transport kinetics via the terrace diffusion mechanism inside the Au-poor phase. We demonstrate the possible generation of Au-rich or Au-poor 2D islands.

II. EXPERIMENTAL

Ge(111) wafers are first cut ($0.5 \times 4 \times 17$ mm^3) and cleaned by acetone and ethanol rinsing before introduction in ultrahigh vacuum (10^{-8} Pa). Then they are cleaned by repeated cycles of ion bombardment (Ar^+, $E = 1$ keV, $I = 8$

[*] frederic.leroy.3@univ-amu.fr

μA) and annealing (1000 K). At last, the crystals are annealed close to the Ge melting point (1211 K) during a few seconds to obtain extended (111) terraces at the surface [14] (>10 μm^2). The electric current is applied in the ⟨110⟩ direction. The sample temperature is adjusted independently from the electric current by using a complementary radiative W filament and an electron bombardment heating stage [30]. The temperature is measured with an Impac pyrometer ($\epsilon = 0.56$) that has been calibrated using the Ge(111)-($\sqrt{3} \times \sqrt{3}$)-Au to -(1 × 1)-Au surface phase transition occurring at 913 K for 1 monolayer (ML) [3] and the eutectic melting point of Au-Ge droplets (634 K). The absolute temperature precision is about 50 K in the range 600–900 K. Au is deposited by evaporation-condensation using an MBE-Komponenten Gmbh effusion cell containing 5N Au shots. We deposit less than 1 ML of Au on Ge(111) to avoid the formation of Au-Ge droplets. Since the solubility of Au into Ge bulk crystal is less than 10^{-4} at. % at the solid state, Au dissolution is negligible [31]. The migration of Au is studied by low energy electron microscopy (LEEM III, Elmitec GmbH) in bright-field mode, with an electron-beam energy of 6.0 eV. Low energy electron diffraction (LEED) patterns are measured at various electron energies in the range 3–30 eV.

III. RESULTS AND DISCUSSION

A. 2D-gas phase of Au on Ge(111): The determination of the Au adatom valence

The LEEM image in Fig. 1(a) shows the surface of a Ge(111) single crystal at 830 K covered with about 0.25 ML of Au under an applied electric current ($j = 1.2 \times 10^6$ A m^{-2}). This surface is obtained after a sharp temperature drop from 900 K. Initially the surface looks homogeneous, i.e., covered with a uniform gas of Au adatoms. After a temporary evolution of less than a minute, the surface reaches a stationary state with smooth intensity variations and no border as expected for a gas phase. The intensity contrast at the surface varies in the direction of the electric current (see movie S1 in the Supplemental Material [32]). It is clear that the downhill step edge of the substrate, perpendicular to the electric current, acts as an Erlich-Schwoebel barrier [3,33,34] such that the Au adatoms cannot cross them easily. Assuming that the intensity contrast is linearly related to the local coverage of the Au adatom gas [29] we can extract the coverage profile of the Au adatoms at the surface [see Fig. 1(b)]. Theoretically we can calculate the stationary coverage profile of the adatom gas from Maxwell-Boltzmann statistics considering an external force on adatoms and an impermeable boundary at the downhill step edge (assuming also that the adatoms do not interact with each other). This coverage profile results from the balance between the flux of adatoms due to the electromigration force and the opposite flux arising from the coverage gradient (Fick's law). The flux of adatoms due to the electromigration force reads $j_{el} = \frac{D c_{\mathrm{Au}}}{k_B T} F$ where D is the Au diffusion coefficient, c_{Au} is the local Au adatom coverage, k_B is the Boltzmann constant, T is the temperature, and $F = eZ^*E$ is the electromigration force (E is the applied electric field and e is the elementary charge). The flux arising from the coverage gradient is $j_c = -D\frac{\partial c_{\mathrm{Au}}}{\partial x}$. Theoretically the

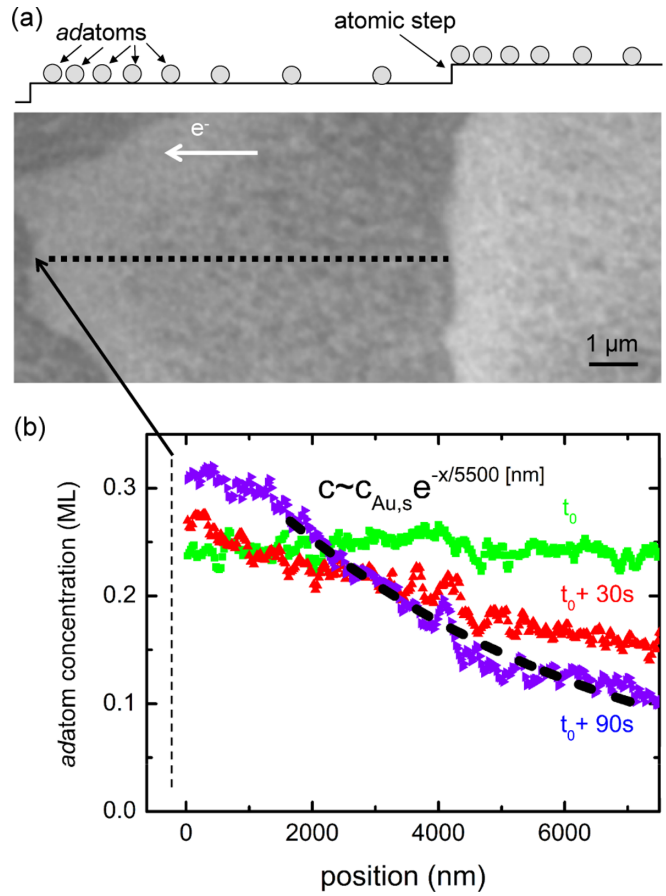

FIG. 1. (a) LEEM image (bright-field mode) of Au (∼0.25 ML) on Ge(111) at 830 K. The black arrows show atomic steps. (b) Coverage profile of Au adatoms extracted from the intensity (corrected from inhomogeneous illumination) along the dashed line of (a). The dashed line corresponds to the best fit of the Au adatom coverage profile using $c(x) = c_{\mathrm{Au},s} e^{\frac{x}{\xi}}$ (see text). $\xi = -5500 \pm 1000$ nm gives the best agreement.

Au adatom gas coverage profile reads

$$c_{\mathrm{Au}} = c_{\mathrm{Au},s} e^{-\frac{\epsilon_p}{k_B T}}, \tag{1}$$

where $c_{\mathrm{Au},s}$ is the maximum Au coverage close to the step edge and $\epsilon_p = -eZ^*E\,x$ is the potential energy of Au adatoms under an electric bias. This potential energy is proportional to the distance x with respect to the maximum of coverage (close to the step). From the experimental profile $c(x) = c_{\mathrm{Au},s} e^{\frac{x}{\xi}}$ we can estimate the electromigration length $\xi = \frac{k_B T}{eZ^*E} = -5500 \pm 1000$ nm [see experimental fit in Fig. 1(b)] and therefore the valence of Au adatoms $Z^* = -82 \pm 15$ ($E = 150$ V/m). The sign of Z^* shows that the Au adatoms displace in the direction of the electron flow. This value is within the range of calculated values for metal adatoms [35–38] and is consistent with a dominant wind force. The calculated force is $F = eZ^*E = (-1.2 \pm 0.2) \times 10^{-5}$ eV/nm = $(-2.0 \pm 0.4) \times 10^{-15}$ N. It acts as a weak perturbation with respect to the random thermal diffusion process ($\frac{Fa}{k_B T} \ll 1$ where a is an atomic distance). Contrary to previous estimates of the valence of atoms that involve mass transfer measurements [39,40] and therefore a prior evaluation of the

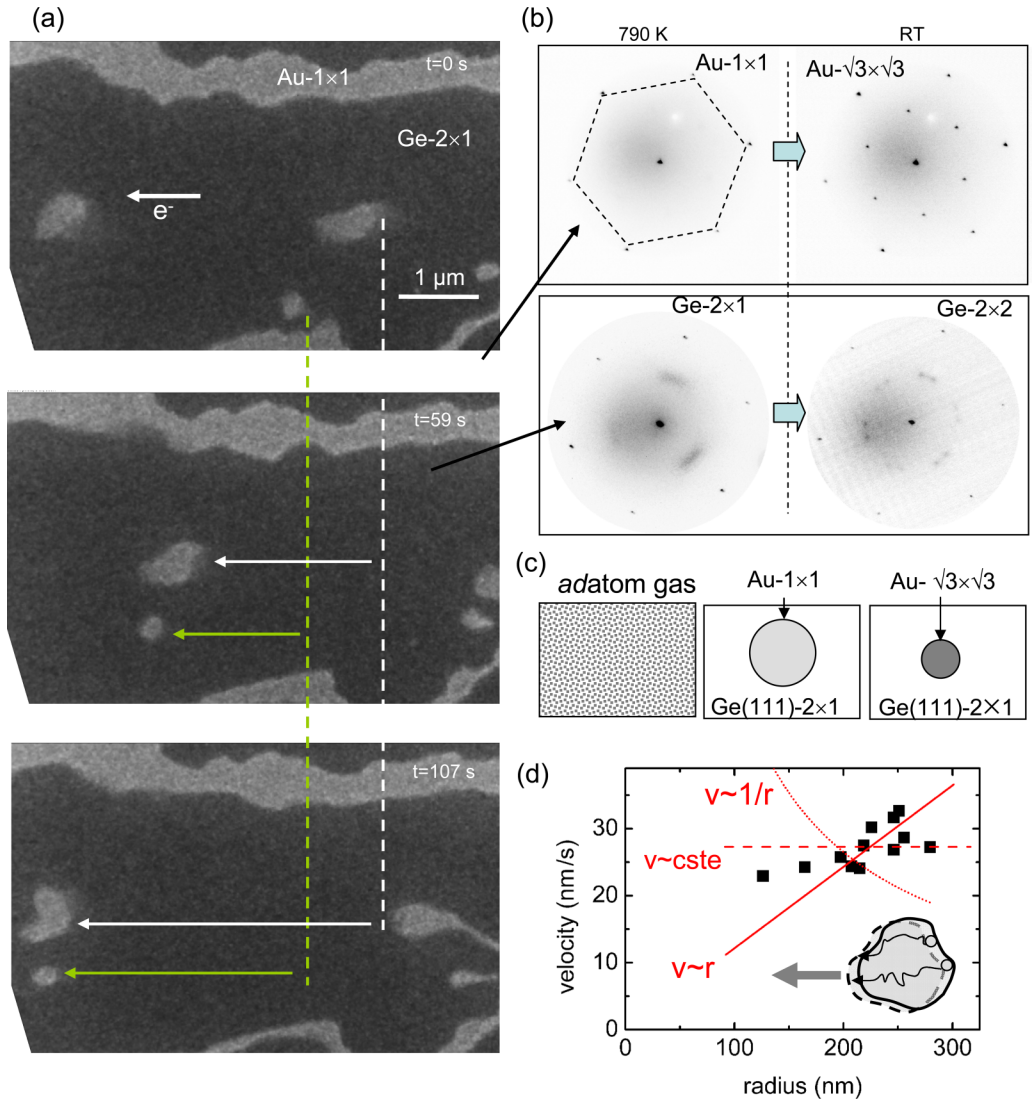

FIG. 2. (a) Series of three LEEM images (bright-field mode) of Ge(111)-(1 × 1)-Au islands electromigrating on Ge(111) at ∼790 K. Ge(111)-(1 × 1)-Au islands have a bright contrast whereas the remaining surface [Ge(111)-(2 × 1)] is darker. The white and green arrows show the displacement of the islands over time. The white arrow indicates the direction of the electron flow. (b) LEED pattern ($E = 14$ eV) of the Ge(111)-(1 × 1)-Au reconstructed islands at 790 K and phase transition into the Ge(111)-($\sqrt{3} \times \sqrt{3}$)-Au at RT. LEED pattern of the Ge(111)-(2 × 1) at 790 K (average projection of 80 LEED patterns between 3 and 14 eV) and phase transition into the split reconstruction Ge(111)-(2 × 2) at RT (LEED at $E = 14$ eV). (c) Schematics of the phase transformation from 2D-gas, Au-poor Ge(111)-(1 × 1)-Au island and Au-rich Ge(111)-($\sqrt{3} \times \sqrt{3}$)-Au phase. (d) Size dependence of the velocity of the Ge(111)-(1 × 1)-Au. The radius is obtained as $\sqrt{A/\pi}$ where A is the island area. Best fit considering different mass transport mechanisms: terrace diffusion (dashed line), periphery diffusion (dotted line), and attachment-detachment (red line). Inset: Schematic of the principle of mass transport by terrace diffusion inside the island.

diffusivity of the entities Dc and/or surface instability modeling [41–44], here it is remarkable that this result involves a straightforward modeling and no free parameter except Z^*.

B. 2D Au-poor phase on Ge(111)

When the temperature is below 800 K and for low Au coverage (below 0.367 ML [3]), the Au adatom gas condenses into 2D islands that electromigrate in the direction of the electron flow [see Figs. 2(a)–2(c)]. The LEED patterns show a Ge(111)-(1 × 1)-Au surface reconstruction for the islands and a diffuse Ge(111)-(2 × 1) reconstruction for the surrounding surface [see Fig. 2(b)]. This latter surface structure occurs on Ge(111) in the presence of remaining Au adatoms at the surface that disorganize the $c(2 \times 8)$ reconstruction of the pure Ge(111) surface [45,46]. The Ge(111)-(2 × 1) reconstruction transforms into a split Ge(111)-(2 × 2) structure [47] at room temperature (RT) and shows a similar LEED pattern as the Ga-induced Ge(111) surface reconstruction [48] [see Fig. 2(b)]. Concerning the Ge(111)-(1 × 1)-Au phase of the islands formed by condensation of the Au adatom gas, it evolves into the Ge(111)-($\sqrt{3} \times \sqrt{3}$)-Au reconstruction at RT [3]. This phase change is accompanied by a strong area shrinking of the islands by a factor ∼3 [see Fig. 2(c)]. As deduced by Giacomo and coworkers [3], the Au coverage inside the Ge(111)-(1 × 1)-Au phase is about 0.367 ML

(the Ge(111)-($\sqrt{3} \times \sqrt{3}$)-Au phase has a Au coverage of 1 ML [49]). We denote in the following the Ge(111)-(1 × 1)-Au [resp. Ge(111)-($\sqrt{3} \times \sqrt{3}$)-Au] surface reconstruction as the Au-poor phase (resp. Au-rich phase).

To determine the mass transport phenomena responsible for the directed migration of the 2D Au-poor islands, size-dependent island velocity measurements have been performed [see Fig. 2(d)]. The island drift velocity is rather size-independent (only a weak velocity increase is measured). Pierre-Louis *et al.* [4] have theoretically studied the island velocity under electromigration in the framework of the linear response theory. The velocity v shows different scaling laws with respect to the island size (r) for different mass transport phenomena: periphery diffusion ($v \sim r^{-1}$), terrace diffusion (v is size-independent), or attachment-detachment at step edges ($v \sim r$). From the fit of the experimental data with the different mass transport phenomena, the dominating one is more likely to be terrace diffusion. Furthermore, since the islands migrate in the same direction as the Au atoms (electron flow), we deduce that the terrace diffusion mechanism occurs within the islands and not from the surrounding surface. This result is in agreement with the low surface density of Au atoms in the Au-poor islands [3] that allows numerous diffusion paths for atoms. Within this framework the 2D-island velocity reads [4]

$$v = \frac{Dc}{k_B T} F = \frac{Dc_{\mathrm{Au}}}{\xi}. \tag{2}$$

Considering a mean island velocity of 26 nm/s [see Fig. 2(c)] we can estimate the Au diffusivity on Ge(111) $Dc_{\mathrm{Au}} = (1.4 \pm 0.4) \times 10^5$ nm^2/s assuming that the effective valence of Au is preserved ($Z^* = -82$).

Furthermore, we observe that the 2D islands exhibit very large shape fluctuations (see Figs. 2(a) and 3(a), and movie S2 in the Supplemental Material [50]). While the area of the islands is approximately fixed, the perimeter exhibits large variations over time [see Fig. 3(b)]. The normalized standard deviation of the perimeter is 15% ± 2%. In addition the mean shape is far from being circular: the ratio of the effective island radius deduced from the perimeter ($r_P = \frac{P}{2\pi}$) and the radius deduced from the area ($r_A = \sqrt{\frac{A}{\pi}}$) is about 2 indicating a strongly noncircular shape (one for a disk). The large shape fluctuations may explain the slight increase of the island velocity with the island size [see Fig. 2(d)].

To quantify these fluctuations and estimate the line tension stiffness $\tilde{\beta}$ that tends to keep the shape compact, we have analyzed the autocorrelation function of a straight edge of a Ge(111)-(1 × 1)-Au domain pushed onto a Ge step [the electric current is perpendicular to the island; see Fig. 3(c)]. Since mass transport is dominated by terrace diffusion as deduced from previous size-dependent velocity measurements, the autocorrelation function $G(t) = \langle [x(y,t) - x(y,0)]^2 \rangle$ of the step edge position is theoretically given by [51]

$$G(t) = 0.86 \left(\frac{\Omega k_B T}{\tilde{\beta}} \right)^{2/3} (2Dc \times t)^{1/3}, \tag{3}$$

where $\Omega = 0.139$ nm^2 is the atomic area. From the fit of the experimental autocorrelation function $G(t) = (810 \pm 250) \times t^{0.33}$ we derive $\tilde{\beta} = 1.2 \pm 0.4$ meV/nm [see Fig. 3(d)]. As expected from the large shape fluctuations, this line tension is vanishingly small, e.g., two orders of magnitude lower than usual step line tensions at the surface of semiconductors (e.g., 600 meV/nm for Si(111) step at ∼1100 K [1]) or metals (e.g., 300–400 meV/nm for Pt(111) step at ∼500 K [51]). It is also consistent with the proximity to the transition temperature of the 2D islands into a 2D Au adatom gas at the Ge surface. Such large fluctuations have also been observed in the context of Pb 2D layers on Ge(111) that fluctuate between two surface phases of similar atomic density [2,3]. However in this case we infer that the fluctuations arise from an extremely small line tension related to the low atomic density of the Ge(111)-(1 × 1)-Au 2D phase ($c_{\mathrm{Au}} \sim 0.367$ ML [3]) that makes the atomic interactions weak.

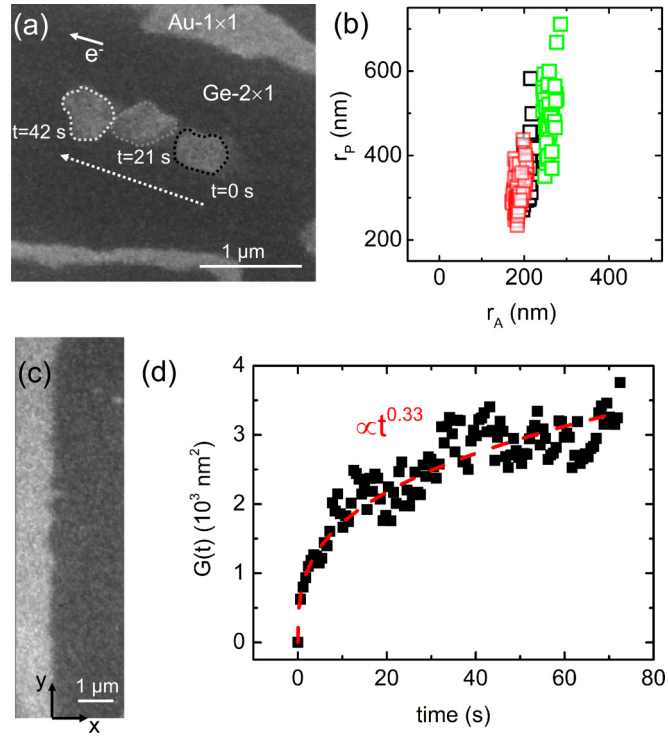

FIG. 3. (a) Projection of three LEEM images measured at $t = 0$, 21, and 42 s. The shape changes are illustrated by dotted contour lines. (b) Plot of the effective island radius r_P deduced from the perimeter versus the effective radius r_A deduced from the island area and considering a circular shape (each color corresponds to an electromigrating island upon ∼50 time steps). While the area is approximately constant, the perimeter shows large variations. (c) LEEM image of an extended Ge(111)-(1 × 1)-Au domain compressed onto a surface step. (d) Time dependence of the autocorrelation function $G(t)$ of the free edge of the domain and fit assuming $G(t) \sim t^{1/3}$.

C. 2D Au island electromigration on Ge(111)

Upon cooling at about 770 K, the Au-poor islands shrink into Au-rich islands, i.e., Ge(111)-($\sqrt{3} \times \sqrt{3}$)-Au islands. The Au-rich islands do not move on the Ge(111)-(2 × 1) surface under the electric bias (velocity detection limit is about 1 nm/s). As it is a Au-rich phase, with a nominal

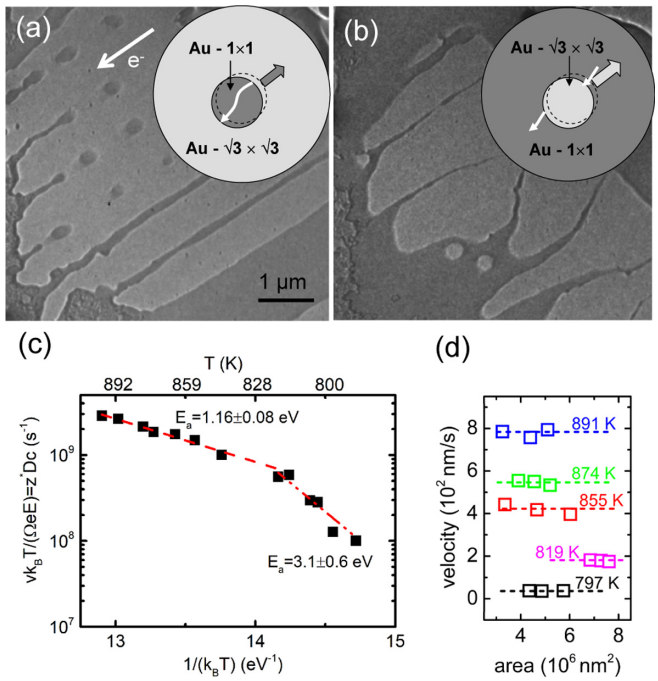

FIG. 4. (a) LEEM image (bright-field mode) of electromigrating Ge(111)-(1 × 1)-Au islands in Ge(111)-($\sqrt{3} \times \sqrt{3}$) phase (scale bar 5 μm). (b) LEEM image (bright-field mode) of electromigrating Ge(111)-($\sqrt{3} \times \sqrt{3}$)-Au islands in Ge(111)-(1 × 1)-Au phase at 830 K. Insets of (a) and (b): Model of mass transfers. (c) Arrhenius plot of the 2D islands $\frac{vk_BT}{\Omega Z^* eE}$. (d) Velocity of islands as function of island size and for different temperatures. At a given temperature, the island velocity is size-independent (dashed guide line).

Au coverage of 1 ML, it does not permit inner mass transport by terrace diffusion, except via vacancies. This reduces drastically the Au-rich island velocity as compared to the velocity of the Au-poor islands. However, at larger Au coverage (0.367 ML $< c_{\mathrm{Au}} <$ 1 ML), the Au-rich and Au-poor phases coexist at the surface and in this case, Fig. 4(a) shows Au-poor islands electromigrating inside the Au-rich phase (see movie S3 in the Supplemental Material [52]). The Au-poor islands are generated regularly at the edge of a large terrace and this process is phenomenologically similar to the generation of bubbles in fluids. The reverse situation also occurs [see Fig. 4(b)]. Size-dependent measurements of the island velocity show that it is strictly independent of the size [see Fig. 4(d)]. In addition the Au-poor and Au-rich phases both electromigrate in the same direction, i.e., opposite to the electron flow. This clearly shows that the Au atoms are moving by terrace diffusion (size-independent velocity argument) inside the Au-poor phase [same direction argument; see models in insets of Figs. 4(a) and 4(b)]. To explain the apparent motion of the Au-rich phase whereas diffusion is strongly hindered inside we have to invoke an interfacial mechanism of phase transformation at the interface between the Au-rich and Au-poor phases. Considering the electromigration of Au-poor islands, the Au-rich phase transforms into the Au-poor phase at the front of the island and vice versa at the back. This phenomenon is kinetically equivalent to an attachment-detachment process. Therefore we can infer that the electromigration of these islands results from a two-step process: (i) terrace diffusion of Au to reach the interface between the two phases and (ii) phase transformation. The size-dependent island velocity measurements indicate that the kinetics of phase transformation is much faster than the timescale for atoms to cross the island by terrace diffusion. Interestingly we can also see that the island shape does not show significant fluctuations. This observation can be related to a large atomic density of the Au-rich phase that imposes a large line tension stiffness at the boundary with the Au-poor phase. Let us note that the absence of shape fluctuations and the size independence of the island velocity reinforce our proposal that the small size dependence of the velocity of the Au-poor islands on the Ge(111)-2 × 1 surface is related to the shape fluctuations. To estimate the activation energy E_a involved in the Au diffusivity ($Dc_{\mathrm{Au}} = D_0 c_0 e^{-\frac{E_a}{k_B T}}$) of the migrating islands ($D_0 c_0$ is a constant prefactor), we have performed island velocity measurements in the temperature range 800–900 K [see Fig. 4(c)]. The islands reach a maximum velocity of about 850 nm/s at 900 K. The Arrhenius plot of $\frac{vk_BT}{\Omega eE} = Z^* Dc_{\mathrm{Au}}$ shows two slops: above 820 K, the activation energy of Au on Ge(111)-(1 × 1)-Au surface is $E_a = 1.16 \pm 0.08$ eV and below 820 K the activation energy strongly increases and reaches $E_a = 3.1 \pm 0.6$ eV. While the small activation energy above 820 K is compatible with atomic diffusion, the large energy barrier below 820 K should involve the surface diffusion of complex species such as small clusters. Nakatsuji and coworkers [53] have shown by scanning tunneling microscopy that there are two typical structures randomly distributed on the Ge(111)-($\sqrt{3} \times \sqrt{3}$)-Au surface: triangle structures and clusters and their density depend strongly on the surface coverage of the Ge(111)-($\sqrt{3} \times \sqrt{3}$)-Au phase and on temperature. Although these experiments were performed at lower temperature, they provide an indication for interpreting the large increase of the activation energy of Au mass transport below 820 K by considering large-size mobile entities such as Au clusters.

IV. CONCLUSION

In conclusion we have studied the electromigration of 2D Au layers on Ge(111) in the range 750–900 K. Depending on the coverage and temperature we have put in evidence the presence of a 2D atomic gas, a Au-poor 2D phase [Ge(111)-(1 × 1)-Au], and a Au-rich 2D phase [Ge(111)-($\sqrt{3} \times \sqrt{3}$)-Au]. The stationary coverage profile of the Au adatom gas phase provides a quantitative estimate of the effective valence of Au atoms ($Z^* = -82 \pm 15$) involved in the electromigration wind force assuming a perfect gas and a strong Erlich-Schwoebel barrier at the step edge. At lower temperature and/or higher Au coverage, the Ge(111)-(1 × 1)-Au phase occurs forming 2D islands that electromigrate in the direction of the electron flow. The weak size dependence of the island velocity indicates a dominant terrace diffusion mechanism of mass transport inside the islands. By addressing the position fluctuations of a straight edge of the Ge(111)-(1 × 1)-Au phase we quantitatively estimate the line tension stiffness. It is vanishingly small due to the weak atomic interactions that perfectly match the low surface density of atoms in this phase. The increase of the Au

coverage allows the coexistence of the dilute Ge(111)-(1 × 1)-Au phase (Au-poor) and a dense Ge(111)-($\sqrt{3} \times \sqrt{3}$)-Au phase (Au-rich). We were able to obtain Au-poor 2D islands migrating into the Au-rich phase and vice versa. The 2D islands electromigrate via diffusion inside the Au-poor phase and phase transformation at the interface with the Au-rich phase. We have shown by size-dependent measurements of the island velocity that the limiting mass transport mechanism is terrace diffusion and the interfacial phase transformation phenomenon does not limit the kinetics of mass transfers. From the Arrhenius plot of the velocity we demonstrate the presence of two regimes: above 820 K, the activation energy involved in the Au diffusivity is 1.16 ± 0.08 eV whereas it increases steeply below and reaches 3.1 ± 0.6 eV. We attribute this change of behavior to a change of diffusing species from Au atoms to small Au clusters respectively at high and low temperature.

ACKNOWLEDGMENTS

This work has been supported by the ANR grant HOLOLEEM (Grant No. ANR-15-CE09-0012). We thank Olivier Pierre-Louis (ILM, Lyon, France) for fruitful discussions on mass transport processes at surfaces.

[1] A. B. Pang, K. L. Man, M. S. Altman, T. J. Stasevich, F. Szalma, and T. L. Einstein, Step line tension and step morphological evolution on the Si(111) (1 × 1) surface, Phys. Rev. B **77**, 115424 (2008).

[2] Y. Sato, S. Chiang, and N. C. Bartelt, Spontaneous Domain Switching during Phase Separation of Pb on Ge(111), Phys. Rev. Lett. **99**, 096103 (2007).

[3] J. A. Giacomo, C. H. Mullet, and S. Chiang, Growth, phase transition, and island motion of Au on Ge(111), J. Chem. Phys. **155**, 054701 (2021).

[4] O. Pierre-Louis and T. L. Einstein, Electromigration of single-layer clusters, Phys. Rev. B **62**, 13697 (2000).

[5] I. A. Blech and E. S. Meieran, Electromigration in thin Al films, J. Appl. Phys. **40**, 485 (1969).

[6] P. S. Ho and T. Kwok, Electromigration in metals, Rep. Prog. Phys. **52**, 301 (1989).

[7] H. Yasunaga and A. Natori, Electromigration on semiconductor surfaces, Surf. Sci. Rep. **15**, 205 (1992).

[8] C. Tao, W. G. Cullen, and E. D. Williams, Visualizing the electron scattering force in nanostructures, Science **328**, 736 (2010).

[9] A. Kumar, D. Dasgupta, C. Dimitrakopoulos, and D. Maroudas, Current-driven nanowire formation on surfaces of crystalline conducting substrates, Appl. Phys. Lett. **108**, 193109 (2016).

[10] A. Kumar, D. Dasgupta, and D. Maroudas, Surface nanopattern formation due to current-induced homoepitaxial nanowire edge instability, Appl. Phys. Lett. **109**, 113106 (2016)

[11] Q. Liu, R. Zou, J. Wu, K. Xu, A. Lu, Y. Bando, D. Golberg, and J. Hu, Molten Au/Ge alloy migration in Ge nanowires, Nano Lett. **15**, 2809 (2015).

[12] S. Curiotto, F. Leroy, F. Cheynis, and P. Müller, Self-propelled motion of Au-Si droplets on Si(111) mediated by monoatomic step dissolution, Surf. Sci. **632**, 1 (2015).

[13] S. Curiotto, F. Leroy, F. Cheynis, and P. Müller, In-plane Si nanowire growth mechanism in absence of external Si flux, Nano Lett. **15**, 4788 (2015).

[14] S. Curiotto, F. Leroy, F. Cheynis, and P. Müller, Surface-dependent scenarios for dissolution-driven motion of growing droplets, Sci. Rep. **7**, 902 (2017).

[15] F. Leroy, P. Müller, J. J. Metois, and O. Pierre-Louis, Vicinal silicon surfaces: From step density wave to faceting, Phys. Rev. B **76**, 045402 (2007).

[16] F. Leroy, D. Karashanova, M. Dufay, J. M. Debierre, T. Frisch, J. J. Metois, and P. Müller, Step bunching to step-meandering transition induced by electromigration on Si(111) vicinal surface, Surf. Sci. **603**, 507 (2009).

[17] S. Curiotto, P. Müller, A. El-Barraj, F. Cheynis, O. Pierre-Louis, and F. Leroy, 2D nanostructure motion on anisotropic surfaces controlled by electromigration, Appl. Surf. Sci. **469**, 463 (2019).

[18] H. B. Huntington and A. R. Grone, Current-induced marker motion in gold wires, J. Phys. Chem. Solids **20**, 76 (1961).

[19] I. A. Blech, Electromigration in thin aluminum films on titanium nitride, J. Appl. Phys. **47**, 1203 (1976).

[20] A. H. Verbruggen, Fundamental questions in the theory of electromigration, IBM J. Res. Dev. **32**, 93 (1988).

[21] S. Curiotto, F. Cheynis, P. Müller, and F. Leroy, 2D manipulation of nanoobjects by perpendicular electric fields: Implications for nanofabrication, ACS Appl. Nano Mater. **3**, 1118 (2020).

[22] F. Leroy, A. El Barraj, F. Cheynis, P. Müller, and S. Curiotto, Electric forces on a confined advacancy island, Phys. Rev. B **102**, 235412 (2020).

[23] A. V. Latyshev, A. L. Aseev, A. B. Krasilnikov, and S. I. Stenin, Transformation on clean Si(111) stepped surface during sublimation, Surf. Sci. **213**, 157 (1989).

[24] Y. Homma, R. J. Mcclelland, and H. Hibino, DC-resistive-heating-induced step bunching on vicinal Si(111), Jpn. J. Appl. Phys. **29**, L2254 (1990).

[25] P. Kuhn, J. Krug, F. Hausser, and A. Voigt, Complex Shape Evolution of Electromigration-Driven Single-Layer Islands, Phys. Rev. Lett. **94**, 166105 (2005).

[26] A. Kumar, D. Dasgupta, and D. Maroudas, Complex Pattern Formation from Current-Driven Dynamics of Single-Layer Homoepitaxial Islands on Crystalline Conducting Substrates, Phys. Rev. Applied **8**, 014035 (2017).

[27] S. Curiotto, F. Leroy, P. Müller, F. Cheynis, M. Michailov, A. El-Barraj, and B. Ranguelov, Shape changes of two-dimensional atomic islands and vacancy clusters diffusing on epitaxial (111) interfaces under the impact of an external force, J. Cryst. Growth **520**, 42 (2019).

[28] F. Cheynis, F. Leroy, A. Ranguis, B. Detailleur, P. Bindzi, C. Veit, W. Bon, and P. Müller, Combining low-energy electron microscopy and scanning probe microscopy techniques for surface science: Development of a novel sample-holder, Rev. Sci. Instrum. **85**, 043705 (2014).

[29] F. Cheynis, S. Curiotto, F. Leroy, and P. Müller, Spatial inhomogeneity and temporal dynamics of a 2D electron gas in interaction with a 2D adatom gas, Sci. Rep. **7**, 10642 (2017).

[30] V. Usov, C. O. Coileain, and I. V. Shvets, Influence of electromigration field on the step bunching process on Si(111), Phys. Rev. B **82**, 153301 (2010).
[31] H. Okamoto and T. B. Massalski, The Au-Ge (gold-germanium) system, Bull. Alloy Phase Diagrams **5**, 601 (1984).
[32] See Supplemental Material at http://link.aps.org/supplemental/10.1103/PhysRevB.106.115402 for the time evolution of Au adatom gas under an electric bias by *in situ* LEEM.
[33] R. L. Schwoebel and E. J. Shipsey, Step motion on crystal surfaces, J. Appl. Phys. **37**, 3682 (1966).
[34] G. Ehrlich and F. G. Hudda, Atomic view of surface self-diffusion: Tungsten on tungsten, J. Chem. Phys. **44**, 1039 (1966).
[35] O. Bondarchuk, W. G. Cullen, M. Degawa, E. D. Williams, T. Bole, and P. J. Rous, Biased Surface Fluctuations due to Current Stress, Phys. Rev. Lett. **99**, 206801 (2007).
[36] P. J. Rous, Electromigration wind force at stepped Al surfaces, Phys. Rev. B **59**, 7719 (1999).
[37] M. F. G. Hedouin and P. J. Rous, Relationship between adatom-induced surface resistivity and the wind force for adatom electromigration: A layer Korringa-Kohn-Rostoker study, Phys. Rev. B **62**, 8473 (2000).
[38] K. H. Bevan, H. Guo, E. D. Williams, and Z. Zhang, First-principles quantum transport theory of the enhanced wind force driving electromigration on Ag(111), Phys. Rev. B **81**, 235416 (2010).
[39] H. Yasunaga, N. J. Wu, S. Yoda, T. Aida, and K. Sakamoto, Atomic layer control by electromigration on semiconductor surfaces, Appl. Surf. Sci. **60-61**, 64 (1992).
[40] M. Degawa, H. Minoda, Y. Tanishiro, and K. Yagi, Direct-current-induced drift direction of silicon adatoms on Si(111)-(1 × 1) surfaces, Surf. Sci. **461**, L528 (2000).
[41] A. V. Latyshev, H. Minoda, Y. Tanishiro, and K. Yagi, Adatom effective charge in morphology evolution on Si(111) surface, Surf. Sci. **401**, 22 (1998).
[42] K. Thürmer, D. J. Liu, E. D. Williams, and J. D. Weeks, Onset of Step Antibanding Instability due to Surface Electromigration, Phys. Rev. Lett. **83**, 5531 (1999).
[43] V. Usov, S. Stoyanov, C. O Coileain, O. Toktarbaiuly, and I. V. Shvets, Antiband instability on vicinal Si(111) under the condition of diffusion-limited sublimation, Phys. Rev. B **86**, 195317 (2012).
[44] E. E. Rodyakina, S. S. Kosolobov, and A. V. Latyshev, Drift of adatoms on the (111) silicon surface under electromigration conditions, JETP Lett. **94**, 147 (2011).
[45] R. S. Becker, B. S. Swartzentruber, J. S. Vickers, and T. Klitsner, Dimer-adatom-stacking-fault (DAS) and non-DAS (111) semiconductor surfaces: A comparison of Ge(111)-C(2 × 8) to Si(111)-(2 × 2), Si(111)-(5 × 5), Si(111)-(7 × 7), and Si(111)-(9 × 9) with scanning tunneling microscopy, Phys. Rev. B **39**, 1633 (1989).
[46] I. Razado-Colambo, Jiangping He, H. M. Zhang, G. V. Hansson, and R. I. G. Uhrberg, Electronic structure of Ge(111)$c(2 \times 8)$: STM, angle-resolved photoemission, and theory, Phys. Rev. B **79**, 205410 (2009).
[47] L. Seehofer and R. L. Johnson, STM study of gold on Ge(111), Surf. Sci. **318**, 21 (1994).
[48] M. Böhringer, P. Molinàs-Mata, J. Zegenhagen, G. Falkenberg, L. Seehofer, L. Lottermoser, R. L. Johnson, and R. Feidenhans'l, Possible mechanism for the room-temperature stabilization of the Ge(111) $T > 300^{\circ}C$ phase by Ga, Phys. Rev. B **52**, 1948 (1995).
[49] P. B. Howes, C. Norris, M. S. Finney, E. Vlieg, and R. G. van Silfhout, Structure of Ge(111)$\sqrt{3} \times \sqrt{3}$ R30°-Au determined by surface x-ray diffraction, Phys. Rev. B **48**, 1632 (1993).
[50] See Supplemental Material at http://link.aps.org/supplemental/10.1103/PhysRevB.106.115402 for the complete movie of the electromigration of Au-poor islands on Ge(111)-1 × 1 surface.
[51] H. C. Jeong and E. D. Williams, Steps on surfaces: Experiment and theory, Surf. Sci. Rep. **34**, 171 (1999).
[52] See Supplemental Material at http://link.aps.org/supplemental/10.1103/PhysRevB.106.115402 for the complete movie of Au-poor islands electromigrating inside the Au-rich phase.
[53] K. Nakatsuji, Y. Motomura, R. Niikura, and F. Komori, Selective doping in a surface band and atomic structures of the Ge(111) ($\sqrt{3} \times \sqrt{3}$)R30°-Au surface, J. Phys.: Condens. Matter **25**, 045007 (2013).

Correction: The previously published Figures 2 and 3 were missing scale bars and have now been replaced with the corrected versions.